Int. J. Solids Structures Vol. 21, No. 9, pp. 977–994, 1985
Printed in Great Britain.

0020–7683/85 $3.00 + .00

TRANSVERSE SHEAR EFFECTS FOR THROUGH-CRACKS IN AN ELASTIC PLATE

W. YANG and L. B. FREUND
Division of Engineering, Brown University, Providence, RI 02912, U.S.A.

(*Received* 27 *February* 1984)

Abstract—The state of stress in a thin elastic plate which contains through-cracks is studied with a view toward assessing the influence of transverse shear on the crack tip stress and deformation fields. Based on the assumption that the through-the-thickness extensional strain is uniform in the thickness direction, a crack tip boundary layer solution is obtained for the tensile opening mode of deformation (mode 1). As anticipated, the generalized plane stress solution prevails everywhere in the plane of the plate except near boundaries. Near points on any smooth boundary, including the crack faces away from the tips, the plane stress solution is only slightly perturbed. Near crack tips, however, a complicated boundary layer is developed. A standard separation of variables approach to the analysis of the boundary layer fails, but an exact solution is found in the form of a real integral. When evaluated, the solution shows a finite lateral contraction at the crack tip (in contrast to the generalized plane stress result), and the inner solution merges smoothly with the plane stress solution at distances from the tip of one-half to three-fourths of the plate thickness, depending on the value of Poisson's ratio. The results are consistent with experiments intended to establish the limitations of the plane stress interpretation of shadow spot data.

1. INTRODUCTION

Stress analysis based on generalized plane stress theory occasionally leads to peculiar results due, in part, to the fact that it is an approximate three-dimensional theory even when the plane stress equations are solved exactly. A typical case is a thin elastic plate which contains through-cracks and which is subjected to edge loads in the plane of the plate. The lateral contraction of the plate at the crack tips is unbounded, according to generalized plane stress theory. Near a crack tip in a plate, the gradients of the in-plane stress components are very large. If the through-the-thickness contraction due to the Poisson effect is allowed to develop without resistance, which is the case in plane stress, then an extremely large gradient in contraction or, equivalently, an extremely large transverse shear strain arises. Associated with this strain, of course, is a transverse shear stress which may be too large in magnitude to permit the basic assumption of plane stress theory. For the case of wave motion in plates, an approach which includes the possibility of a large transverse shear stress, while retaining the simplicity of a two-dimensional model, was introduced by Kane and Mindlin[1] in their work on the high-frequency extensional vibrations of plates.

In the experimental shadow spot method, which has been used extensively to measure the fracture toughness of materials[2, 3, 4], it is this lateral contraction which is measured in order to infer values of the prevailing stress intensity factor. The influence of the deformation near the crack tip on a geometrical light field is interpreted on the basis of plane stress theory. This means of interpreting the data must eventually break down as the points on the specimen which influence the light field become closer and closer to the crack tip, and this analysis is undertaken to provide a quantitative estimate of this restriction.

An initial study of the problem of cracks in plates was made by Sih and Chen[5]. They assumed that a plane strain field prevails very near to the crack tip, and they did not concern themselves with the transition from this field to the plane stress field which must exist at some distance from the tip. In the present article, which is based on the kinematic assumptions which are introduced in [1], the limiting field at the crack tip is of the generalized plane strain type (uniform through-the-thickness extension, rather

than zero through-the-thickness extension in plane strain), and a boundary layer solution is constructed which provides a smooth transition from the near-tip generalized plane strain solution to the near-tip plane stress solution.

In the next section, the governing equations are reduced to two partial differential equations in the plane of the plate for the lateral contraction and the sum of the in-plane normal stress resultants. One equation is a Laplace equation and the other is a Helmholtz equation, and the two equations are coupled through the boundary conditions. The nature of the solution of these equations is then examined, first, for points which are near neither the outer boundary nor a crack surface. Then, the solution is studied for points which are near a boundary but not near a crack tip and, finally, the solution is examined for points which are near a crack tip. As expected, the equations reduce essentially to the plane stress equations in the first case. In the second case (near smooth boundary points), the equations admit a weak ordinary boundary layer solution. On the other hand, for points near crack tips, a complicated boundary layer develops. The governing equations are solved in this region by means of the Wiener–Hopf technique, and a complete description of the transition from generalized plane strain to plane stress is provided along the crack line ahead of the tip. Recent experimental data which focuses on the issue being considered here is included in the last section.

2. GOVERNING EQUATIONS

An elastic plate is bounded by planes $x_3 = \pm h$, where x_i, $i = 1, 2, 3$ represent cartesian coordinates. The outer boundary of the plate is a right cylindrical surface intersecting the plane $x_3 = 0$ in a closed curve Γ_0 and the plate contains n through-cracks with crack surfaces which intersect the plane $x_3 = 0$ in n nonintersecting curves Γ_i, $i = 1, \ldots, n$; see Fig. 1. The kinematic assumption which is basic to this approach is that the displacement field $u_i(x_1, x_2, x_3)$ has the form

$$u_\alpha = v_\alpha(x_1, x_2) \qquad u_3 = x_3 w(x_1, x_2)/h. \tag{1}$$

In (1), and throughout the remainder of the study, Greek indices will have the range 1, 2. Obviously, (1) implies that material lines normal to the mid-plane of the plate in the undeformed state are also normal in the deformed state and that these lines experience uniform extensional strain $w(x_1, x_2)/h$, where $w(x_1, x_2)$ is the out-of-plane displacement of the surface $x_3 = h$ of the plate.

Two-dimensional field equations are obtained by substituting (1) into the three-dimensional field equations, and then integrating with respect to x_3 between the limits $\pm h$. This procedure has been illustrated by Kane and Mindlin[1] in their work on high-frequency extensional vibrations of plates where material inertia has been taken into

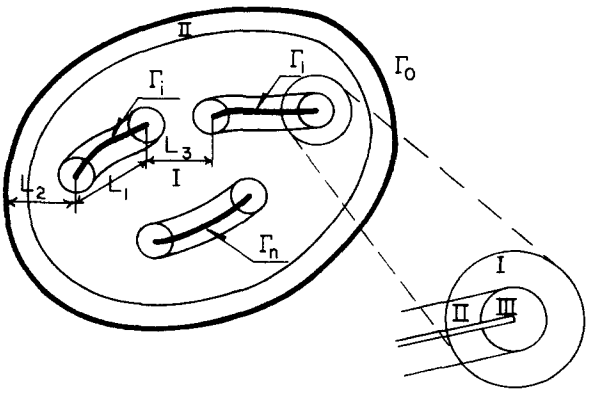

Fig. 1. Geometry and region classification.

account. The system of field equations required here can be obtained from [1] simply by setting the material mass density to zero, and the notation used here is similar to that in [1].

The in-plane stress resultants $N_{\alpha\beta}$ and the transverse shear stress resultants R_α are related to the deformation field (1) through the linear stress-strain law, so that

$$\begin{aligned} N_{\alpha\beta} &= 2h(\lambda\theta\delta_{\alpha\beta} + \mu(v_{\alpha,\beta} + v_{\beta,\alpha})) \\ N_{33} &= 2kh(\lambda\theta + 2\mu kw/h) \\ R_\alpha &= (2h^2/3)\mu w_{,\alpha} \end{aligned} \tag{2}$$

where

$$\theta = v_{\alpha,\alpha} + kw/h. \tag{3}$$

λ and μ are the elastic constants, and k is the shear factor which Kane and Mindlin suggest as $2\sqrt{3}/\pi$. In the absence of the body forces and inertial effects, the equilibrium equations are

$$\begin{aligned} N_{\alpha\beta,\beta} &= 0 \\ R_{\alpha,\alpha} &= N_{33}. \end{aligned} \tag{4}$$

If the mean in-plane stress resultant is denoted by $N = N_{\alpha\alpha}/2$, then the normal stress resultant N_{33} can be expressed in terms of w and N as

$$N_{33} = \frac{k}{\lambda + \mu}[\lambda N + 2k\mu(3\lambda + 2\mu)w]. \tag{5}$$

If R_α and N_{33} are eliminated from the equilibrium equations by means of (2) and (5), respectively, then the relationship

$$\frac{h^2}{3k^2}\frac{\lambda + \mu}{3\lambda + 2\mu}\nabla^2 w - w = \frac{1}{2k\mu}\frac{\lambda}{3\lambda + 2\mu}N \tag{6a}$$

between w and N results. The system of field equations is completed by enforcing strain compatibility to obtain

$$\nabla^2\left(\frac{\lambda + 2\mu}{2k\lambda\mu}N - w\right) = 0. \tag{6b}$$

The nature of the governing equations, which have been reduced to the pair (6a,b), is revealed by introducing a new function w_1 as a linear combination of w and N,

$$w = aN + bw_1, \tag{7}$$

where the two constants a and b are defined by

$$a = \frac{1 - \nu}{\nu}\frac{1}{2k\mu} \qquad b = \frac{1}{\nu(1 + \nu)}\frac{1}{2k\mu}. \tag{8}$$

The eqns (6) then take the form

$$\nabla^2 w_1 = 0 \tag{9}$$

$$\epsilon^2\nabla^2 N - N = w_1 \tag{10}$$

where

$$\epsilon = \sqrt{\frac{1-\nu}{6}}\frac{h}{k} \tag{11}$$

is a parameter whose "smallness" will be exploited in the following perturbation analysis.

It is interesting to note that, for a traction boundary value problem, the in-plane stress resultants $N_{\alpha\beta}$ and the lateral contraction w can be determined separately from the other field variables. In this case, the boundary conditions have the form

$$N_{\xi\eta} = \overline{N}_{\xi\eta} \qquad N_{\eta\eta} = \overline{N}_{\eta\eta}$$
$$w_{,\eta} = \frac{3}{2h^2\mu}\overline{R}_{\eta}, \tag{12}$$

where the barred quantities are specified and where the coordinate system is a right-hand system with ξ measured along the boundary and η in the direction of the outward normal.

3. CLASSIFICATION OF REGIONS

Refer to Fig. 1. The intersection of the outer boundary with the plane $x_3 = 0$ and the intersections of the crack surfaces with the plane $x_3 = 0$ are smooth curves, denoted by Γ_0 and by Γ_i, $i = 1, \ldots, n$, respectively. The length of the ith crack is understood to be the arclength of Γ_i, and suppose that the minimum length over all cracks is L_1. The ligament length of the ith crack is understood to be the infimum of the distance between pairs of points, one on the ith crack Γ_i and the other on the outer boundary Γ_0, and suppose that the minimum ligament length over all cracks is L_2. Finally, the separation distance between the ith crack and the jth crack is understood to be the infimum of the distance between pairs of points, one on the ith crack and the other on the jth crack, and suppose that the minimum separation distance over all pairs of cracks is L_3. Then, a possible characteristic length with respect to which this geometry may be scaled is

$$L = \min\{L_1, L_2, L_3\}. \tag{13}$$

Suppose for the moment that the problem is analyzed by assuming that the state of stress at all points in the plate is generalized plane stress. Then the stress field around each crack edge would be dominated by a term with square-root singular radial dependence and with the plane stress intensity factor as the coefficient. Suppose that the minimum over all cracks of the radius of the region around the crack tip in which this stress intensity factor term dominates the stress field is D. For the analysis to follow, the geometrical conditions

$$\frac{h}{L} \ll 1 \qquad \frac{h}{D} < 0.5 \tag{14}$$

are imposed. The first condition implies that the boundary layers developed adjacent to the crack surfaces or to the outer boundary do not interact, so that the boundary layers can be treated separately. The second condition implies the existence of a K-dominated region surrounding each of the crack tips. The numerical factor 0.5 in the second condition is somewhat arbitrary, but this value is suggested by some of the results to follow.

In the spirit of asymptotic analysis, the domain represented in Fig. 1 may be viewed as being comprised of three different types of regions. The bulk of the region for which points are near neither the outer boundary nor the crack surfaces is labeled as type I. The narrow strips adjacent to the outer boundary and the crack surfaces, but not near to the crack tips, are labeled as region type II. The small regions near the crack tips

where a complicated type of boundary layer develops are labeled as type III. It is important to notice that, under the second assumption of eqn (14), the regions of type III are embraced by annular regions of type I in which the stress field is controlled by the local plane stress intensity factor. These annular regions are subregions of I and are labeled as type I_k.

4. SOLUTION IN THE INTERIOR REGION (TYPE I)

In the interior region of type I, the problem can be solved as a regular perturbation problem, that is, the solution has the form

$$N^I_{\alpha\beta} = \sum_{j=1}^{\infty} \epsilon^j N^{(j)}_{\alpha\beta}(x_1, x_2)$$
$$w^I = \sum_{j=1}^{\infty} \epsilon^j w^{(j)}(x_1, x_2). \tag{15}$$

The governing equations for the terms in the expansions are

$$N^{(j)}_{\alpha\beta,\beta} = 0$$
$$\nabla^2 w^{(j)}_{\mathrm{I}} = 0$$
$$N^{(0)} + w^{(0)}_{\mathrm{I}} = 0 \qquad N^{(1)} + w^{(1)}_{\mathrm{I}} = 0 \tag{16}$$
$$N^{(j+2)} + w^{(j+2)}_{\mathrm{I}} = \nabla^2 N^{(j)} \qquad j = 0, 1, \ldots$$

subject to the boundary conditions

$$N^{(0)}_{\xi\eta} = \bar{N}_{\xi\eta} \qquad N^{(0)}_{\eta\eta} = \bar{N}_{\eta\eta}$$
$$N^{(j)}_{\xi\eta} = -T^{(j)}(\xi) \qquad N^{(j)}_{\eta\eta} = -V^{(j)}(\xi) \qquad j = 1, 2, \ldots \tag{17}$$

where $T^{(j)}$ and $V^{(j)}$ will be specified in the next section. Note that, due to the degeneration of the differential operator, only two boundary conditions can be satisfied. Furthermore, for the traction boundary value problem considered here, the stress resultants in region I are uncoupled from w_1. If $\phi(x_1, x_2)$ is the Airy stress function, then

$$N^{(j)}_{\alpha\beta} = \nabla^2 \phi^{(j)} \delta_{\alpha\beta} - \phi^{(j)}_{,\alpha\beta} \tag{18}$$

and the governing equations become

$$\nabla^4 \phi^{(j)} = 0 \qquad j = 1, 2, \ldots$$
$$\nabla^4 \phi^{(j+2)} = \nabla^6 \phi^{(j)} \qquad j = 0, 1, \ldots \tag{19}$$

where $N^I_{\alpha\beta}$ may be determined uniquely from (17) and (19). In principle, the eqns (17) and (19) may be solved through a step-by-step approach based on analytic function theory. Numerous solutions are available for the leading term and, for purposes of the analysis to follow, these solutions are assumed to be known.

Notice that, after some manipulation on (2), (5), and (7), the out-of-plane stress resultants may be expressed in terms of N as

$$N_{33} = \frac{2k}{\nu} \epsilon^2 \nabla^2 N$$
$$R_\alpha = \frac{2k}{\nu(1-\nu^2)} \epsilon^2 (\epsilon^2 \nabla^2 N - \nu^2 N)_{,\alpha}. \tag{20}$$

The out-of-plane stress resultants are of the order ϵ^2 and thus, a state of plane stress is approximately achieved.

In the subregion I_k, the dominant term of $N_{\alpha\beta}$ is

$$N_{\alpha\beta} = \frac{K}{\sqrt{2\pi r}} f_{\alpha\beta}(\theta) \tag{21}$$

where K is the mode 1 plane stress intensity factor, and $f_{\alpha\beta}(\theta)$ is the well-known universal angular variation of stress for plane elastic crack problems.

5. THE WEAK ORDINARY BOUNDARY LAYER (TYPE II)

In region II, a boundary layer solution $(\mathbf{N}^B, w^B)$ should exist so that the total solution

$$(\mathbf{N}^{II}, w^{II}) = (\mathbf{N}^I, w^I) + (\mathbf{N}^B, w^B) \tag{22}$$

will satisfy the third boundary condition. Note that w_1 satisfies the Laplace equation in all regions, and this equation will not admit a boundary layer type of solution. Thus,

$$w_1^B = 0 \tag{23}$$

and the boundary layer fields are defined by the following system

$$\begin{aligned}
N^B_{\alpha\beta,\beta} &= 0 \\
\epsilon^2 \nabla^2 N^B - N^B &= 0 \\
N^B_{\xi\eta} \mid_\Gamma &= \sum_{j=1}^{\infty} \sigma^j T^{(j)}(\xi) \\
N^B_{\eta\eta} \mid_\Gamma &= \sum_{j=1}^{\infty} \epsilon^j V^{(j)}(\xi) \\
aN^B_{,\eta} \mid_\Gamma &= \frac{3}{2h^2\mu} \bar{R}_\eta - w^I_{,\eta} \\
\lim_{\substack{\epsilon \to 0 \\ \eta > 0}} N^B_{\alpha\beta}(\xi, \eta, \epsilon) &= 0
\end{aligned} \tag{24}$$

where ξ and η are local coordinates along and normal to the boundaries.

The normal coordinate is rescaled according to

$$\hat{\eta} = \eta/\epsilon \tag{25}$$

in region II and, from the equilibrium equations, the asymptotic order of the stress resultants is determined as

$$\begin{aligned}
N^B_{\xi\xi} &= \sum_{j=0}^{\infty} \epsilon^j N^j_{\xi\xi}(\xi, \hat{\eta}) \\
N^B_{\eta\eta} &= \sum_{j=0}^{\infty} \epsilon^{j+2} N^j_{\xi\xi}(\xi, \hat{\eta}) \\
N^B_{\xi\eta} &= \sum_{j=0}^{\infty} \epsilon^{j+1} N^j_{\xi\eta}(\xi, \hat{\eta}) \\
N^B &= \sum_{j=0}^{\infty} \epsilon^j N^j(\xi, \hat{\eta}).
\end{aligned} \tag{26}$$

If the expansions (26) are substituted into eqn (24) and like powers of ϵ are equated, then the following expressions for the stress resultants, correct up to order ϵ^2, are obtained,

$$
\begin{aligned}
N^B_{\xi\xi} &= \left\{ -\frac{\nu}{k}\left(\frac{\bar{R}_\eta}{\epsilon}\right) + \epsilon\frac{2}{a}\dot{w}_I^{(0)} + \epsilon^2\left[\frac{2}{a}\dot{w}_I^{(1)} - \left(1 + 2\frac{\eta}{\epsilon}\right)\frac{\nu}{4k}\left(\frac{\bar{R}''_\eta}{\epsilon}\right)\right]\right\} e^{-\eta/\epsilon} \\
N^B_{\eta\eta} &= \epsilon^2\frac{\nu}{k}\left(\frac{\bar{R}''_\eta}{\epsilon}\right) e^{-\eta/\epsilon} \\
N^B_{\xi\eta} &= \epsilon\left[-\frac{\nu}{k}\left(\frac{\bar{R}''_\eta}{\epsilon}\right) + \epsilon\frac{2}{a}\dot{w}_I^{(0)\prime}\right] e^{-\eta/\epsilon} \\
N^B &= -\left\{\frac{\nu}{2k}\left(\frac{\bar{R}''_\eta}{\epsilon}\right) + \epsilon\frac{1}{a}\dot{w}_I^{(0)} + \epsilon^2\left[\frac{1}{a}\dot{w}_I^{(1)} - \left(1 + \frac{\eta}{\epsilon}\right)\frac{\nu}{4k}\left(\frac{\bar{R}''_\eta}{\epsilon}\right)\right]\right\} e^{-\eta/\epsilon},
\end{aligned}
\tag{27}
$$

where the function $\dot{w}_I^{(i)}$ is defined as

$$
\dot{w}_I^{(i)}(\xi) = \lim_{\eta\to 0^+}\frac{\partial}{\partial\eta} w_I^{(i)}(\xi, \eta) \qquad i = 0, 1. \tag{28}
$$

Recall that $w_I^{(0)}$ is the lateral contraction of the plate according to the generalized plane stress solution in region I. From the last of the conditions listed in eqn (24), the function $T^{(j)}$ and $v^{(j)}$ which appeared in (17) can be determined as

$$
\begin{aligned}
T^{(1)} &= -\frac{\nu}{k}\left(\frac{\bar{R}'_\eta}{\epsilon}\right) & T^{(2)} &= \frac{2}{a}\dot{w}_I^{(0)\prime} \\
V^{(1)} &= 0 & V^{(2)} &= -\frac{\nu}{k}\left(\frac{\bar{R}''_\eta}{\epsilon}\right).
\end{aligned}
\tag{29}
$$

In view of (29), the three leading terms in the interior region I may be determined independently.

For the particular case of traction free crack faces, eqns (29) simplify to

$$
T^{(1)} = 0 \qquad T^{(2)} = \frac{2}{a}\dot{w}_I^{(0)\prime} \qquad V^{(1)} = V^{(2)} = 0 \tag{30}
$$

and the in-plane stress resultants in the boundary layer region II are

$$
\begin{aligned}
N^B_{\xi\xi} &= \frac{2\epsilon}{a}(\dot{w}_I^{(0)} + \epsilon\dot{w}_I^{(1)})e^{-\eta/\epsilon} + 0(\epsilon^3) \\
N^B_{\xi\xi} &= 0(\epsilon^3) \\
N^B_{\xi\eta} &= \epsilon^2\frac{2}{a}\dot{w}_I^{(0)\prime}e^{-\eta/\epsilon} + 0(\epsilon^3).
\end{aligned}
\tag{31}
$$

It is evident from these results that the boundary layer in region II along the traction free crack faces is a weak ordinary boundary layer with stress resultants at most of order ϵ.

6. SOLUTION IN THE CRACK TIP REGION (TYPE III)

In contrast to the boundary layer which develops along the crack faces, the crack tip boundary layer is nonuniform and quite complicated. An attempt at a standard separation of variables approach to determine the crack tip fields fails because it is impossible to satisfy all three boundary conditions with a nontrivial solution. Further-

more, the solution form

$$f = \sum_{i=1}^{n} r^i(\theta) e^{-\lambda_i(\theta) r/\epsilon}, \tag{32}$$

which is commonly used in problems of this general type, does not appear to work in the present case. If the crack tip coordinates are rescaled according to

$$(\hat{x}, \hat{y}) = (x_1, x_2)/\epsilon, \tag{33}$$

however, then the governing equations take the form

$$\begin{aligned} N_{\alpha\beta,\beta} &= 0 \\ \hat{\nabla}^2 w_1 &= 0 \\ \hat{\nabla}^2 N - N &= w_1, \end{aligned} \tag{34}$$

where $\hat{\nabla}$ denotes the two-dimensional Laplacian operator in the rescaled coordinate system. In the limit as ϵ goes to zero, the complicated geometry reduces to that of a semi-infinite crack in an otherwise unbounded body, with the crack lying along the negative $\hat{x}$-axis. In view of the symmetry of the deformation fields associated with mode 1 crack tip deformation, attention is focussed on the half plane $\hat{y} > 0$ with the following boundary conditions on $\hat{y} = 0$

$$\begin{aligned} N_{12} = \frac{\partial w}{\partial \hat{y}} &= 0 \qquad -\infty < \hat{x} + \infty \\ N_{22} &= 0 \qquad -\infty < \hat{x} < 0 \\ \frac{\partial N}{\partial \hat{y}} &= 0 \qquad 0 < \hat{x} < +\infty. \end{aligned} \tag{35}$$

In order to match the crack tip solution in region III to the surrounding plane stress intensity solution in subregion I_k, a matching condition is required [7], and the condition

$$\lim_{R\to\infty} (N_{\alpha\beta}, w) = \lim_{r\to 0} (N^I_{\alpha,\beta}, w^I) = (N^k_{\alpha\beta}, w^k) \tag{36}$$

is employed. A requirement such as (36), which is usually called a Prandtl Matching Condition, implies that the outer limit of the inner solution must equal the inner limit of the outer solution. Furthermore, the order conditions

$$\lim_{R\to 0} N_{\alpha\beta} \sim 0(r^{-1/2}) \qquad \lim_{r\to 0} w \sim 0(1) \tag{37}$$

are enforced at the crack tip. The system of eqns (34–37) can be solved by means of Fourier transform methods and the Wiener-Hopf technique, and the procedure is outlined below.

The Fourier transform of the field variables is defined by the integral

$$\{\hat{N}_{\alpha\beta}(s, \hat{y}), \hat{w}(s, \hat{y})\} = \int_{-\infty}^{\infty} \{N_{\alpha\beta}(x, \hat{y}), w(x, \hat{y})\} e^{-isx}\, dx \tag{38}$$

where s is the transform variable. Application of the transform (38) to the governing equations reduces them to a system of ordinary differential equations in $\hat{y}$, and only solutions which decay exponentially as $\hat{y}$ becomes large are retained as physically

admissible. The form of the transformed field variables is found to be

$$\begin{aligned}
\hat{w} &= aA(\alpha e^{-\beta\hat{y}} - \beta e^{-\alpha\hat{y}}) \\
\hat{N} &= A(\alpha e^{-\beta\hat{y}} + c\beta e^{-\alpha\hat{y}}) \\
\hat{N}_{11} &= \beta A\{2\alpha\beta e^{-\beta\hat{y}} - [2s^2 - c(1 - \alpha\hat{y})]e^{-\alpha\hat{y}}\} \\
\hat{N}_{22} &= A\{-2s^2\alpha e^{-\beta\hat{y}} + \beta[2s^2 + c(1 + \alpha\hat{y})]e^{-\alpha\hat{y}}\} \\
N_{12} &= is\beta\{2\alpha e^{-\beta\hat{y}} - (2\alpha + c\hat{y})e^{-\alpha\hat{y}}\}
\end{aligned} \tag{39}$$

where

$$\begin{aligned}
c &= \nu^{-2} - 1 \\
\alpha &= \lim_{\delta\to 0} \sqrt{s^2 + \delta^2} \qquad \beta = \sqrt{s^2 + 1}
\end{aligned} \tag{40}$$

and the branch cuts of α and β are chosen such that

$$\mathrm{Re}\{\alpha, \beta\} \geq 0$$

everywhere in the complex s-plane.

The function $A(s)$ is determined from the mixed boundary conditions in eqn (35). To this end, the sectionally analytic functions of s

$$\begin{aligned}
H_+(s) &= \int_{-\infty}^{0} \frac{\partial}{\partial\hat{y}} N(\hat{x}, \hat{y})\,|_{\hat{y}=0}\, e^{-is\hat{x}}\, d\hat{x} \\
F_-(s) &= \int_{0}^{\infty} N_{22}(\hat{x}, 0) e^{-is\hat{x}}\, d\hat{x}
\end{aligned} \tag{41}$$

are introduced, where $H_+(s)$ and $F_-(s)$ are analytic in the upper and lower halves, respectively, of the complex s-plane. By means of eqns (39) and (41), the second and third conditions of (34) may be written as

$$\begin{aligned}
A[2s^2(\beta - \alpha) + c\beta] &= F_- \\
A(1 + c)\alpha\beta &= H_+ .
\end{aligned} \tag{42}$$

Upon eliminating $A(s)$, the standard Wiener-Hopf equation

$$Q(s)H_+ = \alpha F_- \tag{43}$$

is obtained, where the transformed "kernel" $Q(s)$ is

$$Q(s) = \lim_{\delta\to 0^+} Q(\delta, s) = \lim_{\delta\to 0_+} \left\{\frac{c}{1 + c}\left[1 + \frac{2}{c}s^2\left(1 - \sqrt{\frac{s^2 + \delta^2}{s^2 + 1}}\right)\right]\right\} \tag{44}$$

with

$$\lim_{|s|\to\infty} Q(s) = 1. \tag{45}$$

The function $Q(\delta, s)$ is analytic and nonzero in the strip $-\delta < Im(s) < \delta$. Consequently, the factorization of Q into a product of sectionally analytic functions

$$Q(s) = Q_+(s)Q_-(s) \tag{46}$$

may be performed formally as

$$\ln Q_{\pm}(s) = \pm \frac{1}{2\pi i} \int_{-\infty}^{\infty} \frac{\ln Q(z)}{z - s} \, . \tag{47}$$

By employing Cauchy's integral theorem, the path of integration in (47) may be deformed to embrace the branch cut along the imaginary axis from $z = i\delta$ to $z = i$ in the z-plane. The resulting contour integral may be converted to a real integral for the factors

$$Q_{\pm}(s) = \exp\left\{ -\frac{1}{\pi} \int_0^1 \omega(t) \frac{dt}{t \pm is} \right\} \tag{48a}$$

where

$$\omega(t) = \tan^{-1}\left\{ \frac{t^3}{\left(\frac{c}{2} - t^2\right)\sqrt{1 - t^2}} \right\} . \tag{48b}$$

It is easy to show that $\omega(t)$ is a continuous and monotonically increasing function with values in the range $0 \leq \omega < \pi/2$ for values of t in the range $0 \leq t < 1$. The function $\alpha(s)$ can also be factored as

$$\begin{aligned} \alpha &= \alpha_+ \alpha_- \\ \alpha_+ &= \sqrt{s + i\delta} \qquad \alpha_- = \sqrt{s - i\delta}. \end{aligned} \tag{49}$$

Following the factorization, (43) may be rewritten as

$$Q_+ H_+ / \alpha_+ = \alpha_- F_- / Q_- = E/(1 + c)$$

where $E(s)$ is an entire function which can be determined with the help of the order conditions in eqn (37). The conditions imply that

$$H_+(s) \sim 0(s^{1/2}) \qquad F_-(s) \sim 0(s^{-1/2})$$

as $| s |$ becomes very large which, through Liouville's theorem on bounded entire functions, implies that $E(s)$ is a constant, say E_0. Thus,

$$A(s) = \frac{E_0}{\beta \alpha_- Q_+} \tag{50}$$

where the constant must be determined to satisfy the matching condition (36).

With the Fourier transforms of the field variables determined, the variables in the physical plane may be determined by means of the Fourier inversion integral

$$\{N_{\alpha\beta}(\hat{x}, \hat{y}), w(\hat{x}, \hat{y})\} = \frac{1}{2\pi} \int_{-\infty}^{\infty} \{\hat{N}_{\alpha\beta}(s, \hat{y}), \hat{w}(s, \hat{y})\} e^{i\hat{x}s} \, ds. \tag{51}$$

By means of Cauchy's theorem and Jordan's lemma of contour integration theory, the path of integration may be deformed to embrace the branch cut running along the imaginary axis in the complex s-plane. That is, the inversion contour runs from $i\infty + 0$ to $i\delta$, around the branch point at $i\delta$, and then from $i\delta$ to $i\infty + 0$; see Fig. 2.

The outer limit of the crack tip solution in region III is determined by means of the steepest descent method which requires expansion of the integrands in (51) only

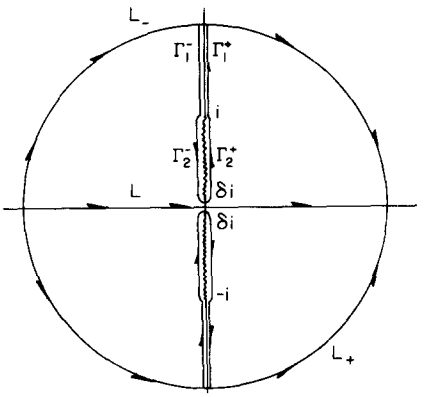

Fig. 2. The integration contour for evaluation of the contour in (51).

for small values of s. From eqns (45) and (46) it is a straightforward matter to show that

$$Q_{\pm}(s) \to \sqrt{1 - \nu^2} \text{ as } | s | \to 0. \tag{52}$$

Thus, the inversion of (51) for large values of r is expressed by the integral

$$\int_{-\infty}^{\infty} \exp \{is\hat{x} - \alpha\hat{y}\}/\alpha_{-} \, ds = 2 \sqrt{\frac{\pi i}{r}} \cos \frac{\theta}{2} \tag{53}$$

and its derivatives. This is a match to the mode 1 plane stress solution in subregion I if and only if the constant E_0 has the value

$$E_0 = \frac{\sqrt{1 - \nu^2}}{c} e^{-i\pi/4} \frac{hK^0}{\sqrt{2\epsilon}}, \tag{54}$$

where K^0 represents the mode 1 stress intensity factor in the plane stress region, subregion I_k. This completes the solution in the crack tip region, that is, the region of type III.

It is of interest to examine the inner solution in region III for points very near to the crack tip, where an expansion of the integrands in (51) for large values of $| s |$ is needed. In view of the results (45) and (53), it is not difficult to show that the stress resultants $N_{\alpha\beta}$ very near to the crack tip in region III have the same angular variation as do the stress resultants in subregion I. Namely,

$$\begin{Bmatrix} N_{11} \\ N_{22} \\ N_{12} \end{Bmatrix} = \frac{hK}{\sqrt{2\pi\epsilon\hat{r}}} \begin{Bmatrix} \cos \frac{\theta}{2} \left(1 - \sin \frac{\theta}{2} \sin \frac{3}{2}\theta\right) \\ \cos \frac{\theta}{2} \left(1 + \sin \frac{\theta}{2} \sin \frac{3}{2}\theta\right) \\ \sin \frac{\theta}{2} \cos \frac{\theta}{2} \cos \frac{3}{2}\theta \end{Bmatrix} \tag{55}$$

as $\hat{r}$ tends to zero. The observation confirms the earlier result by Sih and Chen[5]. Furthermore, the stress intensity factor K in region III can be shown to be related to the plane stress intensity factor in subregion I_k by

$$K = K^0/\sqrt{1 - \nu^2}. \tag{56}$$

This result may be verified by direct application of Rice's path-independent J-integral[6] to the plate geometry.

For point very near to the crack tip in region III, the lateral displacement of the plate surface w can be represented by the integral

$$w \sim \frac{-aE_0}{4\pi} \int_{-\infty}^{\infty} \frac{1 + \alpha\hat{y}}{s^2\alpha_-} e^{-\alpha\hat{y} + is\hat{x}} \, ds, \tag{57}$$

but evaluation of the integral is difficult. However, (6b) and (12) lead directly to the nonhomogeneous Laplace equation and boundary conditions for w,

$$\begin{aligned} \hat{\nabla}^2 w &= a^2 \frac{hK}{\sqrt{2\pi\epsilon\hat{r}}} \cos\frac{\theta}{2} \\ \frac{\partial}{\partial\theta} w(\hat{r}, 0) &= \frac{\partial}{\partial\theta} w(\hat{r}, \pi) = 0. \end{aligned} \tag{58}$$

Application of the method of separation of variables leads to the solution

$$w(\hat{r}, \theta) = w_t + \phi_t \hat{r} \cos\theta + \frac{\nu^2 a}{2\sqrt{1 - \nu^2}} \frac{hK^0}{\sqrt{2\pi\epsilon}} r^{3/2} \left(\cos\frac{1}{2}\theta + \frac{1}{3}\cos\frac{3}{2}\theta \right) + 0(\hat{r}^2) \tag{59}$$

where the constants w_t and ϕ_t represent the lateral displacement of the plate surface and the inclination of the plate surface with respect to the x_1, x_2-plane at the crack tip, that is, at $\hat{r} = 0$. These constants will be determined in the next section.

7. TRANSITION BETWEEN REGION III AND REGION I

From (39) and (51), the surface displacement $w(x, 0)$ and the stress resultant invariant $N(x, 0)$ may be written as

$$\begin{aligned} w(\hat{x}, 0) \equiv w_0 &= \frac{1}{2\pi} \int_{-\infty}^{\infty} aA(\alpha - \beta) e^{i\hat{x}s} \, ds \\ N(\hat{x}, 0) \equiv N_0 &= \frac{1}{2\pi} \int_{-\infty}^{\infty} A(\alpha + c\beta) e^{i\hat{x}s} \, ds. \end{aligned} \tag{60}$$

If the path of integration in (60) is again deformed so as to embrace the branch cut along the imaginary axis in the s-plane, and if the change of variable of integration $s = it$ is introduced, then the integrals in (60) may be written as

$$\begin{aligned} w_0 &= \frac{a\nu^2}{\sqrt{1 - \nu^2}} \frac{hK^0}{\pi\sqrt{2\epsilon}} \left\{ \int_1^{\infty} \frac{t - \sqrt{t^2 - 1}}{\Omega(t)\sqrt{t}\sqrt{t^2 - 1}} e^{-t\hat{x}} \, dt - \int_0^1 \frac{e^{-t\hat{x}}}{\Omega(t)\sqrt{t}} \, dt \right\} \\ N_0 &= \frac{\nu^2}{\sqrt{1 - \nu^2}} \frac{hK^0}{\pi\sqrt{2\epsilon}} \left\{ \int_1^{\infty} \frac{t + c\sqrt{t^2 - 1}}{\Omega(t)\sqrt{t}\sqrt{t^2 - 1}} e^{-t\hat{x}} \, dt + \int_0^1 \frac{ce^{-t\hat{x}}}{\Omega(t)\sqrt{t}} \, dt \right\} \end{aligned} \tag{61}$$

where

$$\Omega(t) = \exp\left\{ -\frac{1}{\pi} \int_0^1 \frac{\omega(\tau)}{t + \tau} \, d\tau \right\}. \tag{62}$$

In order to directly compare the variation of w_0 and N_0 along the x-axis with and without the inclusion of transverse shear effects, the ratios of w_0 and N_0 to their counterparts from a plane stress analysis are calculated based on (61). Following a change of variable

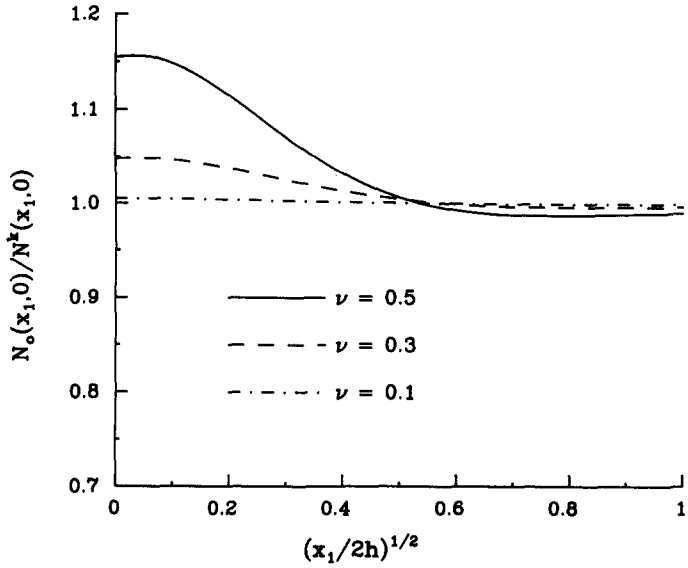

Fig. 3. Mean in-plane stress resultant $N_0(x_1, 0)$ divided by the corresponding value $N^k(x_1, 0)$ for plane stress versus distance ahead of the crack tip from (63) for $\nu = 0.1, 0.3, 0.5$.

of integration intended to result in better properties for numerical evaluation of the integrals,

$$\tilde{w} = \frac{w_0}{w^k(x,0)} = \sqrt{(1-\nu^2)}\frac{\hat{x}}{\pi}\int_0^1 \left\{\frac{2e^{-s^2\hat{x}}}{\Omega(s^2)} + \frac{(s-1)e^{-\hat{x}/\sqrt{1-s^2}}}{(1-s^2)^{5/4}\Omega(1/\sqrt{1-s^2})}\right\} ds$$
$$\tilde{N} = \frac{N_0}{N^k(x,0)} = \sqrt{(1-\nu^2)}\frac{\hat{x}}{\pi}\int_0^1 \left\{\frac{2e^{-\xi\hat{x}}}{\Omega(s^2)} + \frac{\left(s+\frac{1}{c}\right)e^{-\hat{x}/\sqrt{1-s^2}}}{(1-s^2)^{5/4}\Omega(1/\sqrt{1-s^2})}\right\}. \tag{63}$$

The integrands in (63) are free of singularities, provided only that $\hat{x}$ is greater than zero. A standard Gaussian integration scheme is applied to (63) for values of Poisson's ratio of 0.1, 0.3, and 0.5, and the results are shown in Figs. 3 and 4. Several observations can be made on these results. First, the distributions show only a weak dependence on the value of Poisson's ratio. From Fig. 3, it appears that the in-plane stress resultants are relatively insensitive to the transverse shear effects, whereas from Fig. 4 it is clear that the out-of-plane deformation is dramatically affected by transverse shear effects. This latter point is particularly relevant to the experimental shadow spot method[1, 2, 3] which is used to infer values of stress intensity factor by reflection light from the deformed specimen surface near the crack tip and by examining the structure of the reflected optical field. On the other hand, it appears from Figs. 3 and 4 that plane stress results will be sufficiently accurate for points at a distance from the crack tip greater than about $1.0h$ for an incompressible material to $1.5h$ for $\nu = 0.1$.

The same scheme has also been used to calculate w_0/C, namely, the profile of upper plate surface, where

$$C = \frac{av^2h}{\sqrt{1-\nu^2}}\frac{K^0}{\sqrt{2\pi\epsilon}} \tag{64}$$

versus the length/thickness ratio $x_1/2h$. The results are shown in Fig. 5 for the same three values of Poisson's ratio. The important result is that, when transverse shear effects are included, the out-of-plane displacement is finite along the crack edge line. In contrast, according to plane stress results, the out-of-plane displacement is unbounded all along the crack line.

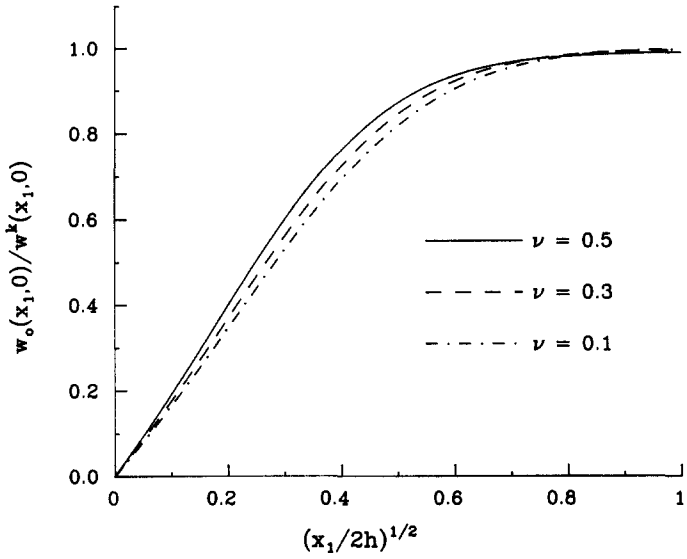

Fig. 4. Lateral contraction $w_0(x_1, 0)$ divided by corresponding value $w^k(x_1, 0)$ for plane stress versus distance ahead of the crack tip from (63) for $\nu = 0.1, 0.3, 0.5$.

To gain some insight into the transition of field type from generalized plane strain at the crack tip to generalized plane stress at more distance points, consider the following property of the function $\Omega(t)$,

$$\text{Max}\left\{\sqrt{1-\nu^2}, \sqrt{\frac{t_1}{1+t_1}}\right\} \leq \Omega(t_1) < \Omega(t_2) \leq 1 \qquad 0 \leq t_1 < t_2 < +\infty, \quad (65)$$

where the second lower bound is in effect when t_1 is greater than c. The property (65) can be proved by means of eqn (48). It has been shown by direct calculation for several values of Poisson's ratio [8] that (65) provides very tight bounds on the function.

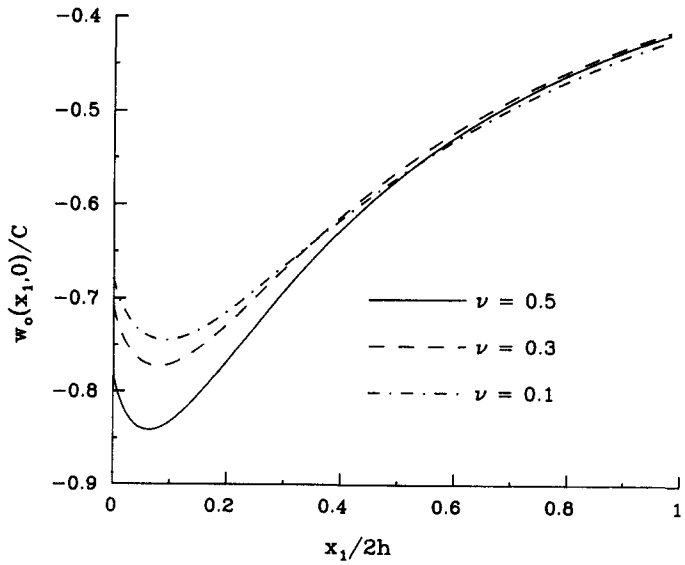

Fig. 5. Lateral contraction versus distance ahead of crack tip ($\nu = 0.1, 0.3, 0.5$) where C is given by (64).

In view of the constant-like behavior of $\Omega(t)$, the mean value theorem may be applied to the integrals in (63) to obtain approximate single integral representations for the field variables $\tilde{w}$ and $\tilde{N}$,

$$\begin{aligned} \tilde{w} &\cong \frac{\sqrt{1-\nu^2}}{\bar{\Omega}}\left(1 - B(\hat{x})\right) \\ \tilde{N} &\cong \frac{\sqrt{1-\nu^2}}{\bar{\Omega}}\left(1 + \frac{1}{c}B(\hat{x})\right) \end{aligned} \tag{66}$$

where $\bar{\Omega}$ is the mean value of $\Omega(t)$ and $B(x)$ is defined by

$$B(\hat{x}) = \frac{1}{\sqrt{\pi}}\int_{\hat{x}}^{\infty} \frac{\sqrt{t}}{\sqrt{t^2 - \hat{x}^2}} e^{-t}\, dt. \tag{67}$$

The function $B(\hat{x})$ is readily identified as a boundary layer type of function and, in fact, it has the property

$$\frac{1}{\sqrt{2}} e^{-\hat{x}} \leq B(\hat{x}) \leq e^{-\hat{x}} \qquad 0 \leq \hat{x} < \infty. \tag{68}$$

The results of a numerical evaluation of the integral definition of B leads to the observation that B varies monotonically, and it tends to its lower (upper) bound as $\hat{x}$ tends to infinity (zero)[8].

Finally, the behavior of w_0 along the positive x-axis is examined in some detail. From (66), w_0 is given approximately by

$$w_0 = \frac{w_R}{\sqrt{\hat{x}}}\{1 - B(\hat{x})\} \tag{69}$$

where

$$w_R = 2^{-7/4}\bar{Y}(\nu)\frac{K^0\sqrt{h}}{\mu} \qquad \bar{Y}(\nu) = \frac{\nu(1-\nu)^{1/4}}{\bar{\Omega}(\nu)\sqrt{1+\nu}} \tag{70}$$

is the "reference contraction." The normalized contraction w_0/W may be evaluated numerically without difficulty by means of the integral

$$\frac{w_0}{w_R} = \frac{1}{\sqrt{\pi}}\left\{\int_0^{\pi/2} \frac{\sqrt{\sin\theta}}{1+\cos\theta} e^{-\hat{x}/\sin\theta}\, d\theta - 2\int_0^1 e^{-s^2 x}\, ds\right\}, \tag{71}$$

and the result is shown in Fig. 6. The results for generalized plane strain very near to the crack tip and for plane stress far from the crack tip are also shown in the same figure for comparison purposes. The undetermined constants w_t and ϕ_t introduced in (59) can also be evaluated from (71) as

$$\begin{aligned} \frac{w_t}{w_R} &= \frac{1}{\sqrt{\pi}}\left\{\int_0^{\pi/2} \frac{\sqrt{\sin\theta}}{1+\cos\theta}\, d\theta - 2\right\} \cong -0.67598 \\ \frac{\phi_t}{w_R} &= \frac{1}{\sqrt{\pi}}\left\{\frac{2}{3} - \int_0^{\pi/2} \frac{(\sin\theta)^{-1/2}}{1+\cos\theta}\, d\theta\right\} \cong 0.49294. \end{aligned} \tag{72}$$

The numerical results indicate that the average function $\bar{\Omega}(\nu)$ could be taken as $\sqrt{1-\nu^2}$ with only a slight error for the near-tip calculations. Therefore, for points

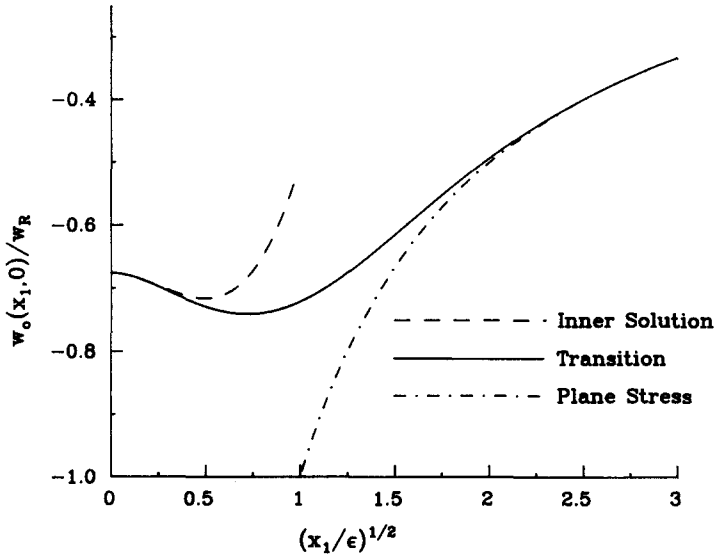

Fig. 6. Lateral contraction ahead of tip, showing inner boundary layer, transition, and outer plane stress regions. The parameter ϵ is defined in (11).

very near to the crack tip, the lateral contraction of the plate may be written as

$$w = \frac{1}{4}\left(\frac{2}{1-\nu}\right)^{1/4}\frac{\nu}{1+\nu}\frac{K_0\sqrt{h}}{\mu}\left\{-0.67598 - 0.49294r\cos\theta + \frac{1}{2}\hat{r}^{3/2}\left(\cos\frac{\theta}{2} + \frac{1}{3}\cos\frac{3}{2}\theta\right)\right\} + 0(\hat{r}^2). \quad (73)$$

This solution does not exhibit plane strain behavior very near to the crack tip as is commonly assumed in problems of this type.

The minimum value of w_0 occurs at $x = x_0$ where

$$w_0'(x_0) = 0.$$

If this condition is imposed on the expression for w_0 in (69), then the following equation for x_0 emerges,

$$\int_{x_0}^{\infty}\frac{t^{3/2}}{\sqrt{t^2 - x_0^2}}e^{-t}\,dt = \frac{\sqrt{\pi}}{2}. \quad (74)$$

The extraneous solution at $x_0 = 0$ is eliminated by multiplying both sides of (74) by $(x_0)^{-3/2}$. The solution is then found to be

$$x_0 \cong 0.5104, \quad (75)$$

and w_0 takes on the minimum value

$$w_{\min} \cong 0.7443 w_R. \quad (76)$$

8. THE OPTICAL SHADOW SPOT MEASUREMENT METHOD

Consider a planar fracture specimen in the single-edge-notch configuration which is loaded in such a way as to produce deformations of the tensile opening type (mode

1). Suppose that nonlinear material response is confined to a very small neighborhood of the crack edge (small scale yielding) and that, for points at a sufficient distance from the crack tip, the mechanical fields are adequately characterized by the theory of plane stress elasticity. Under the action of the applied loads, the specimen undergoes nonuniform thinning, with the through-the-thickness contraction being greatest near the crack tip. If the lateral face of the specimen was initially planar and of high optical reflectivity, then the deformed specimen face is a nonplanar reflecting surface. If parallel light rays are directed normally onto the deformed reflecting surface, then the reflected rays will deviate from parallelism. That is, the reflected light field will have some geometrical structure (when viewed on a plane parallel to the specimen plane, say), and the general idea is to relate this structure to the deformation of the specimen near the crack tip. According to plane stress theory, the deformation of the specimen is completely characterized by the elastic stress intensity factor for points near the crack tip, so that the prevailing value of stress intensity factor may be related directly to an observable dimension in the reflected light field.

If the reflected light rays are gathered by a camera which is focused on a suitable plane behind the specimen, then the photograph produced will show a dark ovoid (region devoid of light rays) surrounded by an illuminated region. The ovoid is the so-called shadow spot, and the level of the stress intensity factor can be shown to be proportional to the maximum transverse diameter of the spot to the power 5/2. The proportionality factor depends on the various lengths of the laboratory set-up, the thickness and elastic properties of the specimen material, and on the instantaneous crack tip speed for dynamic growth. Loosely speaking, the shadow spot arises from the fact that light rays which strike the specimen surface both inside of and outside of a particular curve (the initial curve) are reflected onto the image plane outside of a corresponding curve. This optical reflection process is reviewed in a recent article[9]. The size of the initial curve compared to other dimensions in the system is of central importance in the interpretation of data.

The shadow spot method has several features which make it very attractive for use in fracture mechanics experiments: it is a direct crack tip measurement and thus avoids the complexities of analyzing the stress wave propagation and reflection in the entire specimen to interpret the data; the optical procedure does not interfere with the process being observed; and the response of the optical system is virtually instantaneous on the time scale of mechanical processes. The main disadvantage of the method is that it provides only a surface observation, and the extent to which the surface response of the specimen represents the internal response is somewhat uncertain.

The task of establishing the limitation of the plane stress interpretation of shadow spot data in fracture mechanics experiments has been undertaken by Rosakis and Ravi-Chandar[10]. They prepared compact tension specimens with sharp, planar straight-fronted cracks. The specimens were then loaded to produce a mode 1 deformation field. Then, with a fixed level of load, shadow spot data were taken for initial curves of various sizes by adjusting the optical arrangements used in the experiments. Preliminary results from their experiments are shown in Fig. 7. The figure includes results (solid

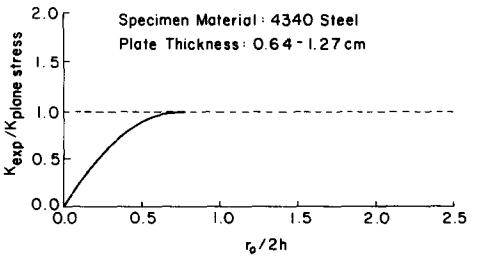

Fig. 7. Ratio of stress intensity factor inferred from shadow spot data to analytical plane stress value versus initial curve radius divided by specimen thickness (from Rosakis and Ravi-Chandar[10]). The solid line is a best-fit curve of their data.

curve) for specimens of a high strength steel of three thicknesses between 0.64 cm and 1.27 cm. The abscissa is the size of the initial curve on the specimen (which is a circle for plane stress) divided by the specimen thickness. The ordinate is the ratio of the experimental value of inferred stress intensity factor to the corresponding analytical value. The analytical value of stress intensity factor is determined from the geometry of the specimen and the magnitude of the applied load on the basis of a plane stress analysis. Likewise, the experimental value is inferred from the shadow spot data on the basis of a plane stress near tip field. For initial curves which pass through points on the specimen which are in regions where plane stress theory provides an accurate description of the deformation field, the ratio of these two stress intensity factor values should be one. It is clear from these data that the plane stress interpretation remains valid for initial curve radii greater than about 50% of the specimen thickness, but that an error of increasing magnitude is introduced if the initial curve is taken closer and closer to the crack tip. The restriction to initial curves greater than about 50% of the specimen thickness agrees extremely well with the results of the present analysis (cf. Fig. 4).

Acknowledgement—We are grateful to Prof. A. J. Rosakis of the California Institute of Technology and Prof. K. Ravi-Chandar of the University of Houston for providing the data shown in Fig. 7 prior to publication of their work.

The research support of the National Science Foundation, Solid Mechanics Program, is gratefully acknowledged. The computations were performed on the VAX-11/780 Engineering Computer Facility at Brown University. This Facility was made possible by grants from the National Science Foundation (Solid Mechanics Program), the General Electric Foundation and the Digital Equipment Corporation.

REFERENCES

1. T. R. Kane and R. D. Mindlin, High frequency extensional vibration of plates, *J. Applied Mech.* **23**, 277–283 (1956).
2. P. Manogg, Anwendungen der schattenoptik zur untersuchung des zerreissvorgangs von platten, Dissertationsschrift an der Universitat Freiburg (1964).
3. P. S. Theocaris, Local yielding around a crack tip in plexiglass, *J. Applied Mech.* **37**, 409–415 (1970).
4. A. J. Rosakis, Analysis of the optical method of caustics for dynamic crack propagation, *Engng Fracture Mech.* **13**, 331–347 (1980).
5. G. C. Sih and E. P. Chen, Dynamic analysis of cracked plates in bending and extension. *Mechanics of Fracture*, Vol. 4 (Edited by G. C. Sih). Noordhoff, Leyden, Netherlands (1977).
6. J. R. Rice, A path independent integral and the approximate analysis of strain concentration by notches and cracks, *J. Applied Mech.* **35**, 379–386 (1968).
7. M. Van Dyke, *Perturbation Methods in Fluid Mechanics*, Parabolic Press, Palo Alto, CA (1975).
8. W. Yang and L. B. Freund, Transverse shear effects for through-cracks in an elastic plate, *Brown University Technical Report* (1983).
9. A. J. Rosakis, C. C. Ma and L. B. Freund, Analysis of the optical shadow spot method for a tensile crack in a power-law hardening material, *J. Applied Mech.* **50**, 777–782 (1983).
10. A. J. Rosakis and K. Ravi-Chandar, private communication, November 1983.